OSM 2018 (PS44A-2261)

Spectral descriptions of coastal submesoscale surface currents and chlorophyll concentrations in an observational view

Sung Yong Kim[1,†], Jang Gon Yoo[1], E. A. Lee[1], and Hyeon Seong Kim[2]

[1]Environmental Fluid Mechanics Laboratory, Department of Mechanical Engineering, Korea Advanced Institute of Science and Technology, 291 Daehak-ro, Yuseong-gu, Daejeon 34141, Republic of Korea

[2] Sun Young Engineering, Co. LTD, 762-4 Haengsin-dong, Deokyang-gu, Goyang-si, Gyeonggi-do, 10486 Republic of Korea

syongkim@kaist.ac.kr[†]

Abstract

Submesoscale coastal surface currents and chlorophyll concentrations at hourly and O(1)-km resolutions, obtained from an array of high-frequency radars and geostationary ocean color imagery in a coastal region off the east coast of Korea over a period of one year (2013), are described in the wavenumber domain (k). The kinetic energy (KE) spectra of the surface currents become steeper at a scale of approximately 10 km from a slope of k-5/3 to slopes between k-2 and k-3 at a length scale of 2 km and exhibit anisotropy which can be associated with the influence of anisotropic coastal boundaries (e.g., the shoreline and bathymetry) and weak seasonality that may result from persistent regional circulations and mixed layer depths modulated by seasonal super-harmonic frequencies. Moreover, the energy spectra of the chlorophyll exhibit anisotropy associated with bathymetric effects and regional circulation, and their decay slopes change from k-5/3 to k-1 at O(10) km scales and from k-1 to k-3 at O(1) km scales. The spectral decay slopes of these energy spectra are consistent with the two-dimensional quasi-geostrophic turbulence theory, and their weak seasonality can be interpreted with the baroclinic instability in the weak seasonal mixed layer under the persistent and non-seasonal regional circulations.

Observations

Hourly averaged observations of surface currents were obtained off the coast of Imwon, Republic of Korea, on a grid with a 1-km spatial resolution over a period of one year (2013) using two phased-array HFRs [WEllen RAdar (WERA) systems] – Imwon North (IMWN; R1) and Imwon South (IMWS; R2) (Figure 1c). For the OI method in this paper, an exponential correlation function with an isotropic decorrelation length scale of 1.5 km and a search radius of 3 km under the cutoff correlation of 0.1 is applied to minimize spatial smoothing on the radial velocity maps with resolutions of at least 1 km.

Hourly GOCI-derived L2A products, including maps of chlorophyll, the colored dissolved organic matter (CDOM), and the total suspended solid (TSS) concentrations; concentration-derived vector currents; and eight-band images around the Korean Peninsula with a spatial resolution of 0.5 km during daylight hours (e.g., maximum of eight snapshots a day) serve as passive mode observations.

Variance in the wavenumber domain

The one-year-averaged wavenumber domain energy spectra of the observed surface currents have decay slopes between k^{-2} and k^{-3} at a scale of 2 km (Figures 2a and 2c), with slight differences in the sampling directions (e.g., the cross-shore and along-shore directions). The seasonally averaged wavenumber domain energy spectra show that their decay slopes are nearly identical in two seasons and that their variances are higher in summer than they are in winter (Figure 2d). The variance of the seasonally averaged energy spectra is also dependent on the sampling directions (Figures 2c and 2d). The wavenumber domain energy spectra of the radial velocities at IMWS have similar decay slopes in their averaged estimates over the year and seasons (not shown), and the number of vector current maps participating in the estimates of the spectral decay slopes does not show any seasonal bias (Figure 2g).

The time series of the estimated spectral decay slopes over the one year are close to the decay slopes of $k^{-5/3}$ and k^{-3} for the individual wavenumber ranges of k_1 and k_2, respectively (Figures 2c and 2d), and they have fluctuations of seasonal super-harmonic variability (Figures 2e and 2f).

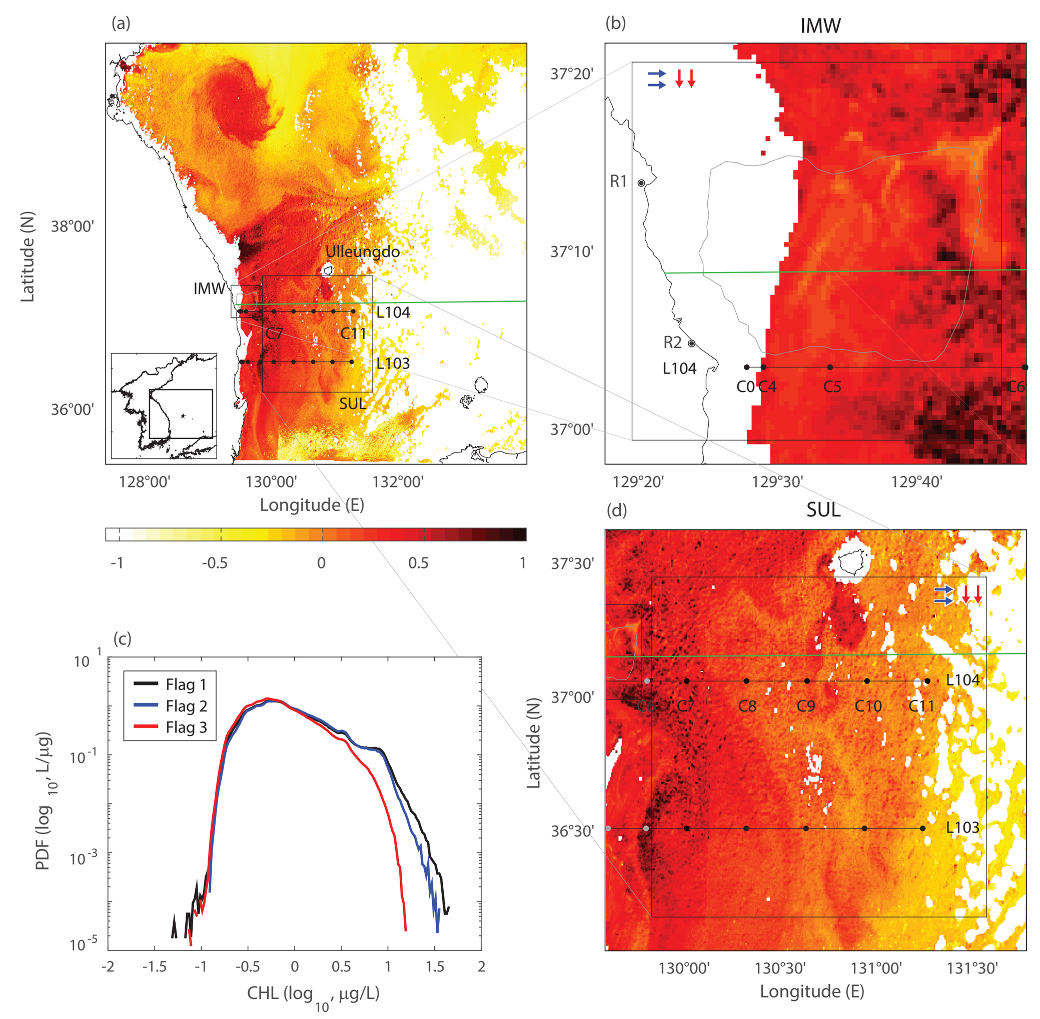

Figure 1: (a) An example of the GOCI-derived chlorophyll concentration ($\log_{10}$, μg L^{-1}) off the East/Japan Sea (EJS), sampled on October 12, 2013. A coastal region (Imwon; IMW) and an open ocean area (South of Ulleungdo; SUL) are marked with black boxes. Stations (C0 to C11) on two hydrographic survey lines (L103 and L104) to sample temperature, density, and nutrients are denoted. A cross-shore green line is chosen to examine seasonal variability of chlorophyll concentrations, relevant drivers. (b) and (d): Close-up of two sub-domains [(b) IMW and (d) SUL]. The effective spatial coverage of HFR-derived surface currents is shown with a gray contour in Figures 1a and 1b. (c) Probability density functions (PDFs) of hourly chlorophyll concentrations ($\log_{10}$, μg L^{-1}) in Figure 1b for a period of five years (2011 to 2015) in terms of the internal QAQC parameters (Flag1, Flag2, and Flag3).

The wavenumber domain energy spectra [$Q_{c1}(k)$ and $Q_{c2}(k)$] of the chlorophyll concentrations sampled in the coastal region (IMW) show consistent spectral decay slopes of k^{-1} ($\lambda > \lambda_D$; $\lambda_D = 3$ km) and $k^{\leq -3}$ ($\lambda \leq \lambda_D$) in both cross-shore and along-shore directions (Figure 3a). In the same region, the KE spectra of the (surface) currents have spectral decay slopes between k^{-2} and k^{-3} at a scale of 2 km [e.g., [1]]. These two submesoscale observations of the chlorophyll concentrations and surface currents can be explained by either QG theory or turbulent flows under geostrophic bathymetric effects, which have spectral decay slopes of k^{-3} and $k^{-2.5}$ at a scale of O(1) km, respectively [e.g., [2]]. The energy spectra of the chlorophyll concentrations in the cross-shore and along-shore directions are consistent, but not identical (Figure 3a). The spatial anisotropy in this region has been reported in the surface current observations as a result of the circulation bounded by the coastal boundaries [e.g., [1]]. Although the observations of the chlorophyll concentrations are limited within the study domain, particularly in the summer (June and July) (Figure 3g), the chlorophyll data sampled from a slightly offshore domain show consistent spectral decay slopes and anisotropy with greater statistical significance, as well as having a greater number of realizations (Figures 3b and 3h). The time series of the spectral decay slopes in the forward cascade region ($\lambda > \lambda_D$) exhibits seasonality and fluctuations at seasonal super-harmonic frequencies, shown as k^{-2} for the summer and k^{-1} for the winter (Figures 3c, 3d, 3e, and 3f). These spectral decay slopes may be explained with the regional baroclinic instabilities within the moderate seasonal MLDs associated with the submesoscale eddies and circulations influenced by coastal boundaries [e.g., [1]]. Conversely, the spectral decay slopes below the dissipation scale ($\lambda \leq \lambda_D$) appear to be nearly out of phase those in the forward cascade region and have weak seasonality (Figures 3c, 3d, 3e, and 3f).

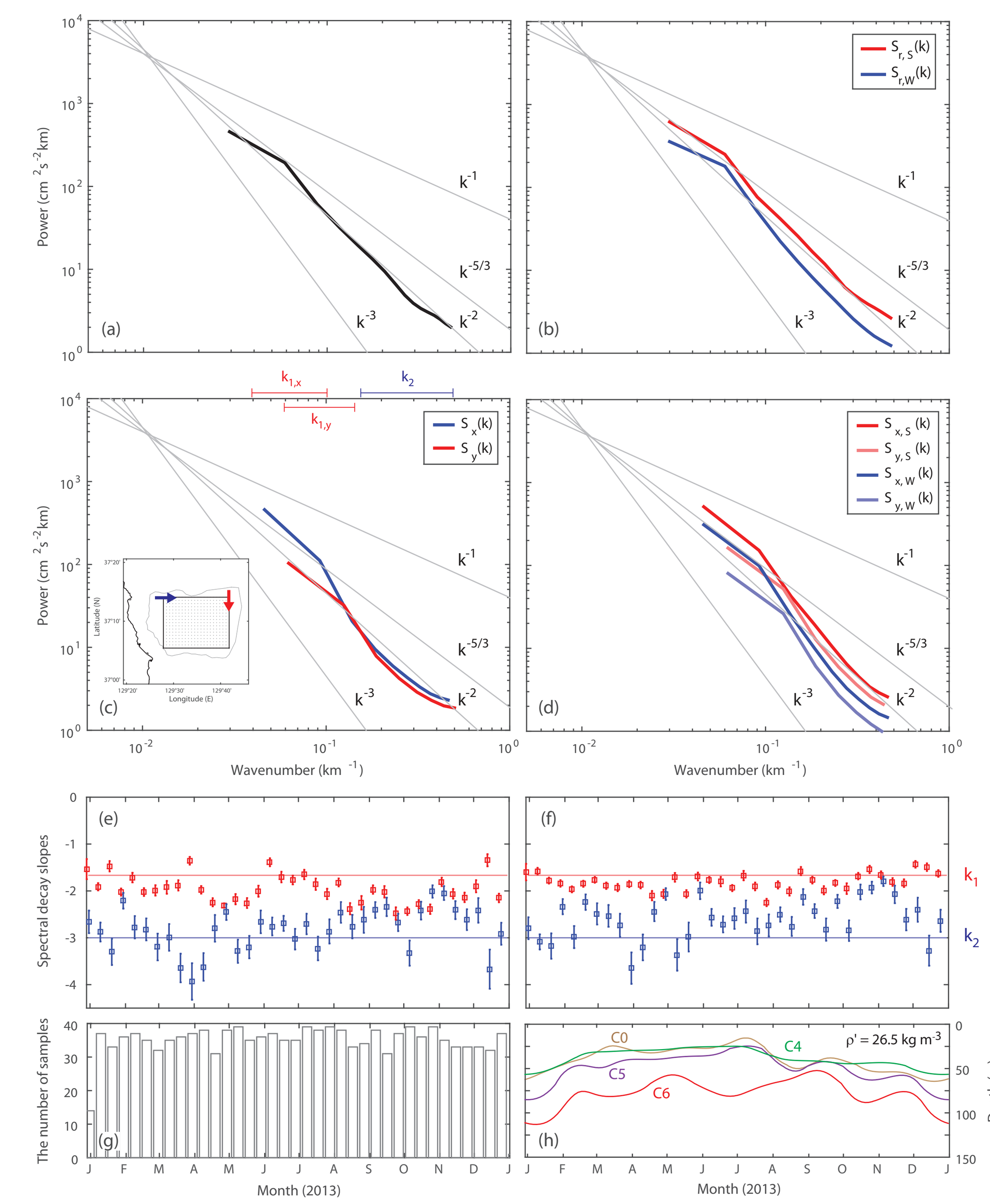

Figure 2: (a) and (b): Wavenumber domain energy spectra of the hourly radial velocities sampled in the range direction at IMWN for a period of one year (2013) are averaged over the entire year (black) and seasons [$S_{r,S}(k)$ for summer (red; June, July, and August of 2013) and $S_{r,W}(k)$ for winter (blue; January, February, and December of 2013)]. The wavenumber domain energy spectra of the radial velocities sampled in the range direction are averaged over in the azimuthal direction. (c) and (d): Wavenumber domain energy spectra of the hourly vector currents for a period of one year (2013) are averaged over the entire year [$S_x(k)$ for cross-shore direction (blue) and $S_y(k)$ for along-shore direction (red)] and seasons [$S_{x,S}(k)$ (red) and $S_{y,S}(k)$ (light red) for summer; $S_{x,W}(k)$ (blue) and $S_{y,W}(k)$ (light blue) for winter]. Gray axillary lines of the spectral decay slopes of k^{-1}, $k^{-5/3}$, k^{-2}, and k^{-3} are overlaid. (e) Spectral decay slopes of $S_x(k)$. (f) Spectral decay slopes of $S_y(k)$. (g) The number of vector current maps participating in the estimates of the spectral decay slopes (The bin size is equal to 10 days). (h) Time series of the depth of the constant density anomaly ($\rho' = 26.5$ kg m^{-3}.

The GOCI-derived chlorophyll concentrations sampled in the open ocean (SUL) exhibit spectral decay slopes of $k^{-5/3}$ ($\lambda > \lambda_I$, $\lambda_I = 10$ km), k^{-1} ($\lambda_D < \lambda \leq \lambda_I$), and $k^{\leq -3}$ ($\lambda \leq \lambda_D$) based on their wavenumber domain energy spectra [$Q_o(k)$] in both the cross-shore and along-shore directions (Figure 4a). These spectral decay slopes can be interpreted as (1) the forward cascades of enstrophy (the integral of the square of the vorticity) and inverse cascades of energy appear at the injection scale [$\lambda_I = O(10)$ km], where the baroclinic instability in the mixed layer (see above) plays a more dominant role as the driver of the submesoscale processes rather than the mesoscale eddy-derived surface frontogenesis does at a scale of O(100) km [e.g., [3]] and (2) the surface dissipation scale appears near O(1) km. Note that the KE spectra of the HFR-derived surface currents do not clearly show the dissipation scale due to limited spatial scale of the observations ($\lambda \geq 2$ km) [[1]]. Similarly, the MODIS- and VIIRS-derived chlorophyll concentrations sampled in the same region have nearly consistent variance of their energy spectra and spectral decay slopes at spatial scales greater than 30 km in the forward cascade region (Figures 4a and 4b). Note that the spectral decay slopes in both directions are nearly identical and differ at length scales of less than 5 km (Figure 4a), which shows the length scale that characterizes the anisotropy.

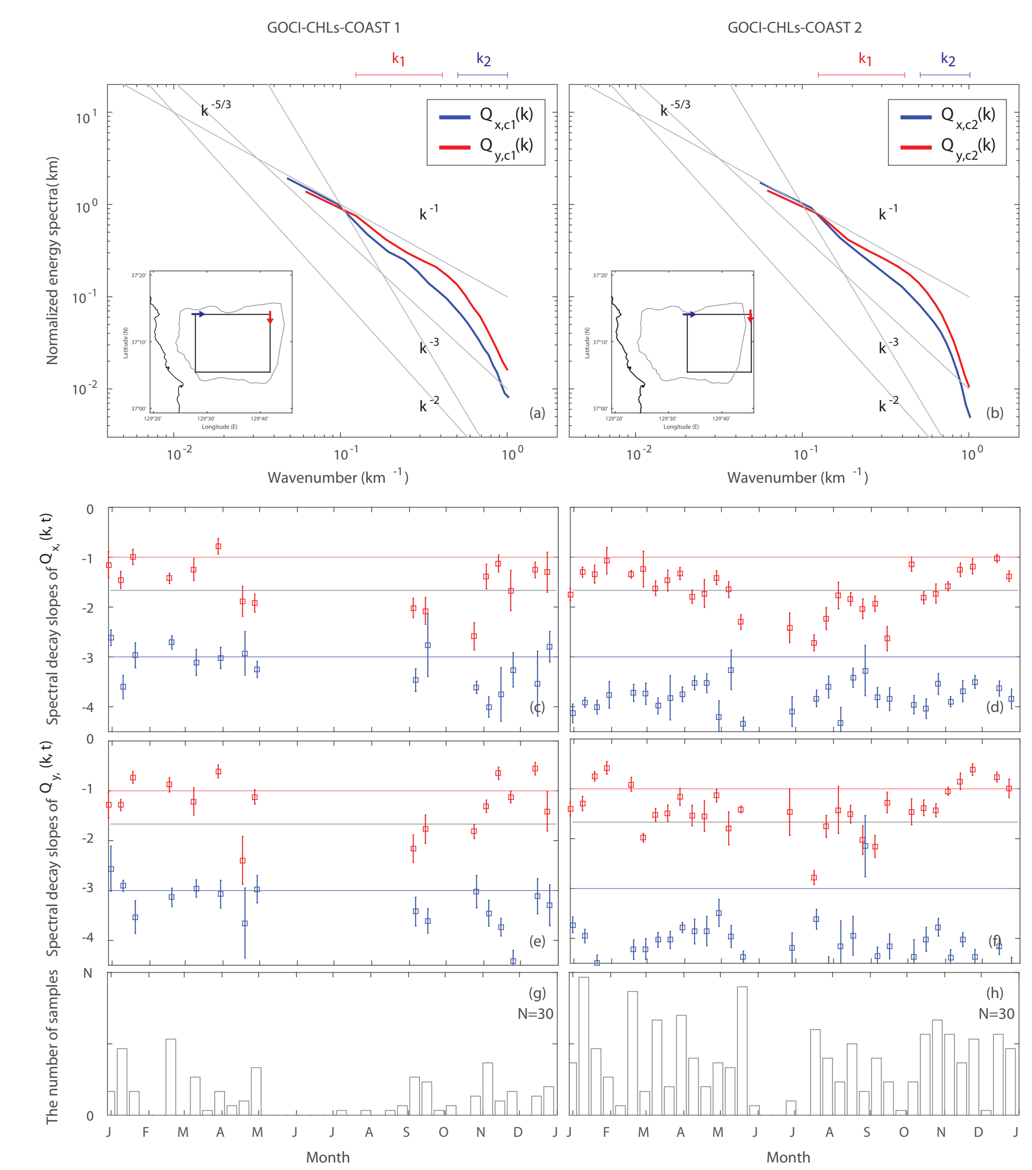

Figure 3: (a) and (b): Wavenumber domain energy spectra of GOCI-derived normalized chlorophyll concentration for a period of five years (2011 to 2015) in two coastal regions – (a) an area completely overlapped with HFR-derive surface currents [$\mathcal{Q}_{c1}(k)$, IMW] and (b) an area off 35 km from the coast [$\mathcal{Q}_{c2}(k)$, IMW]. (c) and (d): Spectral decay slopes of $\mathcal{Q}_x(k,t)$. (e) and (f): Spectral decay slopes of $\mathcal{Q}_y(k,t)$. The temporal mean and standard errors of the estimated spectral decay slopes are 10-daily bin-averaged and presented with a colored square and vertical line, respectively. The expected spectral decay slopes [k^{-1} (red), $k^{-5/3}$ (black), and k^{-3} (blue)] are marked with colored horizontal lines. (g) and (h): The number of chlorophyll concentration maps participating in estimating the spectral decay slope of the energy spectra. The bin size is equal to 10 days. The maximum range (N) of individual histograms is noted. (g) and (h): $N = 30$.

Similarly, based on the energy spectra of the open ocean chlorophyll concentrations, the spectral decay slopes in the forward cascade ($\lambda > \lambda_I$; k_0 and k_0^*) and inverse cascade ($\lambda_D \leq \lambda < \lambda_I$; k_1) show seasonality (Figures 4c to 4f). The spectral decay slopes below the dissipation scale ($\lambda \leq \lambda_D$; k_2) are slightly out of phase with those within the two wavenumber ranges (k_0, k_0^*, and k_1) (Figures 4c and 4e). The amount of data used in the estimates of the energy spectra is not uniformly distributed, which may lead to temporal biases toward January, February, June, July, November, and December (Figures 4g to 4i). Excluding the estimates in these time periods, the spectral decay slopes have fluctuations at the seasonal frequency and its super-harmonic frequencies and become steeper in the summer and flatter inthe winter (Figures 4c to 4f).

In three-dimensional turbulence, the dissipation scale appears at O(1) cm, which can be associated with molecular dissipation. In contrast, in two-dimensional turbulent flows, the dissipation scale is related to the scales at which the gravity waves start to break; three-dimensional effects become important at scales of $O(1-100)$ m [e.g., [4]]. Thus, the surface dissipation scale appears near O(1) km, which can be an upper bound of the observations analyzed in this paper [[5]].

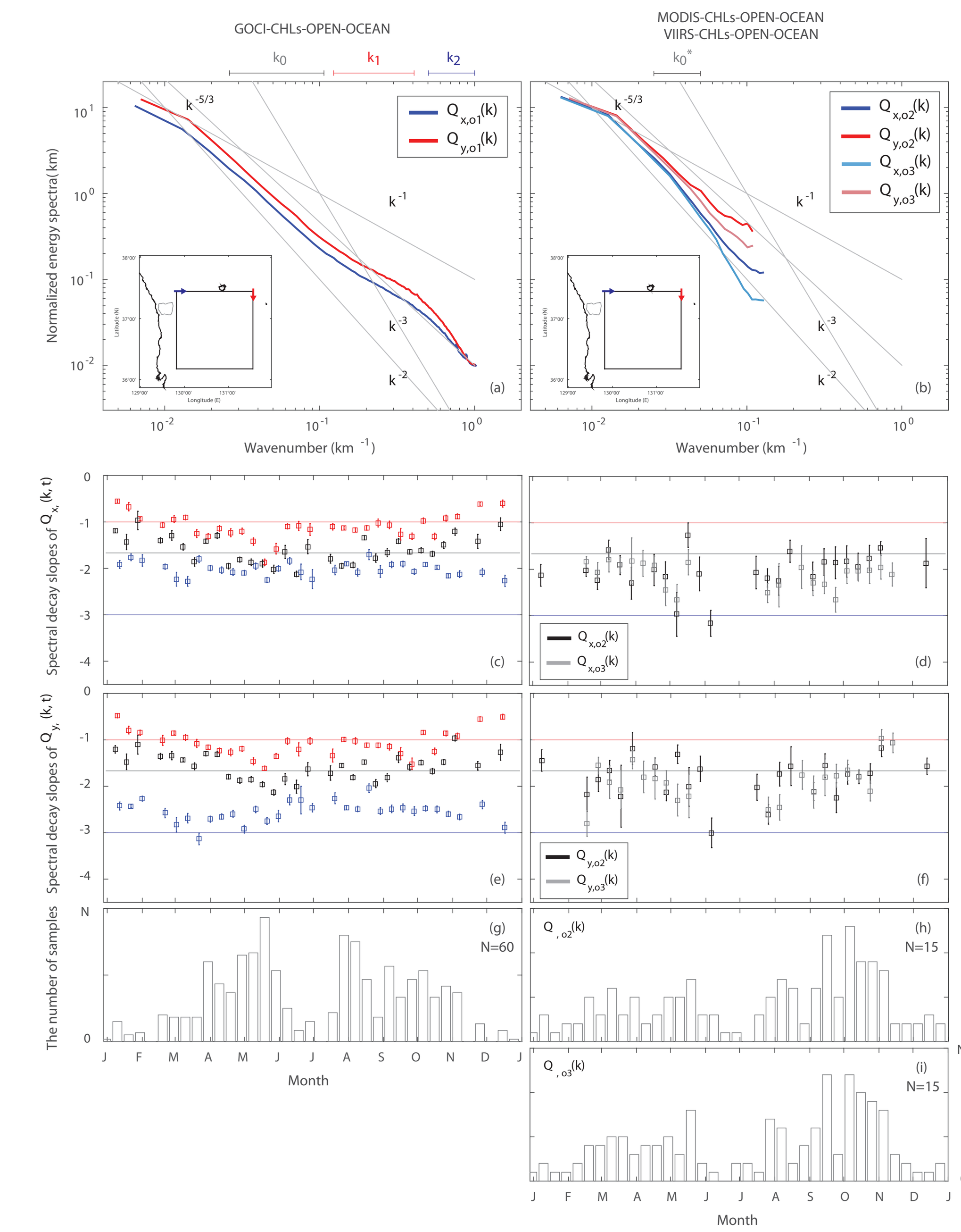

Figure 4: (a) and (b): Wavenumber domain energy spectra of normalized chlorophyll concentrations for a period of five years (011 to 2015) in the open ocean area [$\mathcal{Q}_o(k)$, SUL]. (a) GOCI-derived chlorophyll concentrations [2011 to 2015; $\mathcal{Q}_{o1}(k)$]. (b) MODIS-derived chlorophyll concentrations [2011 to 2015; $\mathcal{Q}_{o2}(k)$] and VIIRS-derived chlorophyll concentrations [2012 to 2015; $\mathcal{Q}_{o3}(k)$]. (c) and (d): Spectral decay slopes of $\mathcal{Q}_x(k,t)$. (e) and (f): Spectral decay slopes of $\mathcal{Q}_y(k,t)$. (g) to (i): The number of chlorophyll concentration maps participating in estimating the spectral decay slope of the energy spectra in Figures 4e and 4f. The bin size is equal to 10 days. The maximum range (N) of individual histograms is noted. (g) $N = 60$. (h) and (i): $N = 15$.

Acknowledgement

This project is supported by a research project titled by a research project titled by 'Research for Applications of Geostationary Ocean Color Imager' through Korea Institute of Marine Science and Technology Promotion (KIMST), Ministry of Oceans and Fisheries and a grant through the Disaster and Safety Management Institute, Ministry of Public Safety and Security (KCG-01-2017-05), Republic of Korea.

References

[1] J. G. Yoo, S. Y. Kim, and H. S. Kim. Spectral descriptions of submesoscale surface circulation in a coastal region. *J. Geophys. Res.*, 2018. submitted.

[2] G. K. Vallis. *Atmospheric and Oceanic Fluid Dynamics*. Cambridge University Press, Cambridge, U.K., 2006.

[3] Ross Tulloch, John Marshall, Chris Hill, and K Shafer Smith. Scales, growth rates, and spectral fluxes of baroclinic instability in the ocean. *J. Phys. Oceanogr.*, 41(6):1057–1076, 2011.

[4] M Nikurashin, GK Vallis, and A Adcroft. Routes to energy dissipation for geostrophic flows in the Southern Ocean. *Nature Geosci.*, 6(1):48–51, 2013.

[5] E. A. Lee and S. Y. Kim. Regional variability and turbulent characteristics of the satellite-sensed submesoscale surface chlorophyll. *J. Geophys. Res.*, 2018. submitted.